Periodicals of Engineering and Natural Sciences ISSN 2303-4521
Vol. 8, No. 3, August 2020, pp.1767-1785

Strain analysis at flat surfaces of loaded members using digital image correlation technique

Mohanad Nazhan Mohammed, Zaid S. Hammoudi, Dhia A. Alazawi
Department of Mechanical Engineering, University of Diyala

ABSTRACT

This research examines the applicability of the planned Digital Image Correlation (DIC) system to measure the strains in tensile experiments. DIC is a low-cost optical technique, and is an appropriate measurement used to measure surface displacement, strain and stress map distribution without any contact with the tested surfaces. In the present research, the tensile test is conducted on two different flat samples, which are painted in a speckle pattern on the tested surface to use DIC features in stain measurements. To guarantee the efficiency of the planned DIC system, the DIC code has been built using MATLAB programming language. The obtained results from DIC technique is compared with the results from open-source software (Ncorr), the finite element analysis (ANSYS) as well as the exact and analytical solutions. The comparison results showed that there was A quite acceptable and agreement achieved between them. According to the exact solution, the percentage of accuracy of the obtained results for the Aluminum without hole plate was around (89-93) % whereas the accuracy with the NCORR was about 96 %. For the second copper plate with a central hole, the accuracy has been obtained to be (80.7-99) % with the analytical solution wherein its value has reached (81-97) % with Ncorr software.

Keywords: Digital image correlation (DIC), dynamic strain, stress, MATLAB code, Aluminum, copper plate, Ncorr software

Corresponding Author:
Mohanad Nazhan Mohammed
Department of Mechanical Engineering, University of Diyala, Diyala – Iraq.
E-mail: mohanadnazhan@gmail.com

1. Introduction

Reliable stress and strain measurement are often required as part of component and sample assessment in various engineering fields. Stress measurement has abroad applications such as the distinguish between alloy deformation mechanisms, tensile loads on the immediate shift of stress in super-elastic alloys, and residual stresses on creeping crack growth in steel, etc. [1-4].

The popular methods for measuring strain are diffraction analyses, including neutron diffraction and X-ray diffraction (XRD). The diffraction analysis coupled with mechanical testing had used in the study of various metals and alloys [5-6].

Numerous strategies had been proposed within full-field displacement and, strain measurements such as speckle pattern, holographic interferometry, geometric moiré, speckle photography and DIC [8].

Each of the used methods to obtain the full-field displacement and strain measurements has become the primary interest in the scientific fields among the other improved experimental techniques in the mechanical tests [7].

DIC represents a non-contact optical method that is used to measure the full-field displacements, strain, and stress. The captured images of the tested specimen have considered as an input to the developed program. The specimen considered in DIC technique might be in different forms such as too small, big, complex, soft, cold, or hot. Hence, this technique can be used inside or outside the laboratory [9].

DIC technique is an optical technique that uses the mathematical context to correlate images, examine the data and evaluate the results of the samples. This technique requires a series of images of a sample. When the sample

is under an incremental load, DIC examines the sample's surface changes and behaviour. the samples are needed to be painted in a random dot pattern (speckle pattern) in this technique as well [10].
In DIC technique with a single camera, it only provides in-plane displacement/strain fields on flat/planner objects whereas using a pair of cameras can estimate the 3-D displacement and strain fields of any 3-D object [11].
This study is in general focuses on building a DIC program, carry out experiments, evaluation for image analysis to find the full-field measurements in the mechanical tests as well as validate the results regarding to the numerical simulation software like ANSYS.
J. Cirne, et al [12], investigated the full-field displacements, strain and stress measurement methods (and their rates). The tensile test had been applied on a splitting Hopkinson bar. The results and measurements were performed using the ARAMIS software. The stated DIC system has two single digital high-speed cameras which give and offer the synchronization. Apparently, this analysis mainly depends on counting the number of pixels of images under the test. The used DIC system can record the frames at a rate of up to 250,000 / second by using the stereo cameras. In contrast, our current work presented in this paper investigates the applicability of DIC to measure full-field displacements, strain and stress measurement using DIC technique. This technique is based on the concept of a searching algorithm to execute image correlation. Single-camera has been used to capture images, Nikon D3200 has been used with shooting rate by 1 frame per second (fps) to 4 fps.
Jean-Jose' Orteu [13], proposed a stereovision technique which experimentally uses two cameras as measurement of 3-D displacement/strain fields on any 3-D object. The paper proved that the stereovision technique is a non-contact method used for the calculations of 3-D displacement, strain and stress fields of any 3-D specimen in industrial applications. This technique is useful in many applications used in large and small scale of structural mechanical problems, and definitely for small and large structures. Our current paper concentrates on performing DIC code to study the functionality of this technique and carry out the measurements on image series taken from the mechanical testing. In this context, only 2D DIC problem has been considered.
S. Kut [14], tested ductile fracture of strain measurements technique, for the sample of the circular cross-section offered by Finite Element Method (FEM) theory. For steel, copper and aluminium tested samples, each obtained result dealing with the ductile fractures. Strains in various fractures positions has been estimated and compared in terms of each sample and another. While the current research presented in our paper has used two rectangular flat samples, first was a copper plate with a central hole and second was aluminium plate without hole. FEM principle also has been used to build the DIC code algorithm.
Shilpa Chakinala [15], the results of the full-field displacement and strain had been computed by a method of subpixel resolution by using sub-pixel DIC algorithms. The researchers in [15] had presented three sub-pixel DIC algorithms that is used in calculations which is most suitable for an implemented experiment. In our paper presented here, the DIC method that is related to the greyscale correlation is indispensable to have at least two images of different experimental states of objects. The captured images have been transformed into a greyscale images by means of using the developed program. The correlation considered 2D cross-correlation analysis, which was applied to perform the technique correlation by computing the scale of submatrices formed between the reference image and the deformed image.
Po-Chih H. and A. S. Voloshin [16], proposed a "fast and simple" (FAS) algorithm that relay on DIC technique to measure the planner sample surface deformation. The future algorithm practices the satisfactory correlation at the pixel especially the resolution and surface scanning for sub-pixel level. There are two individual specimens were examined to find the probability of the planned algorithm. On the contrary, in this current paper, the written DIC code principle is based on finding the grayscale correlation coefficient. This correlation gives a satisfactory relationship between distorted and undistorted sub-images for estimating the distortion of sub-image shown in Figure 1. The correlation coefficient is well-defined as eq (2).
Ellon Bernardes de Assis and Francisco Evangelista Junior [17], had implemented DIC routine to calculate in-plane displacements and strain field. The algorithm achieved an accuracy of 95%. The results in the mentioned paper had taken into consideration the systematic error within the displacement and strain measurements due to the grey-level interpolation. The authors used an interpolation to get the desired results and it was interesting. In our current research presented in this paper, the results of the numerical and experimental investigation are considered. The results that had been discussed in this paper, used to obtain the full-field displacements, strain, and further the stress of each one of the tested specimens. The validity of the results had checked, ANSYS had mainly been used for this purpose. Besides, other open sources DIC software (Ncorr) has been used. Eq (16) is used to compute the percentage of accuracy. The minimum (80.7%) and maximum (99%) accuracy values were achieved. The grey-level interpolation has not been used in this paper.

2. Fundamental theory

This work considers DIC technique to measure the surface deformation by tracking an image feature. With this technique, the entire surface is measured and this represents the full field required measurement. Subsequently, the output of the deformed full-field measurements is involved in many applications. Furthermore, the full-field displacements, strain and stress measurements gained from this technique can be used to validate the finite element simulations and characterize materials, etc. [18]. Some of these measurements are used for characterizing materials by using DIC, VFM (Virtual Fields Methods) and FEMU Finite Element Model Updating [19] [20].

Images of the specimen at zero loads (reference image) and deformed image with one different second load state are required in DIC technique. These images are compared among each other using the developed program as can be seen in Figure 1. The comparison and correlation is carried out using 2D cross-correlation analysis so as to correlate the scale sub matrices between the reference image and the deformed image [21] [22].

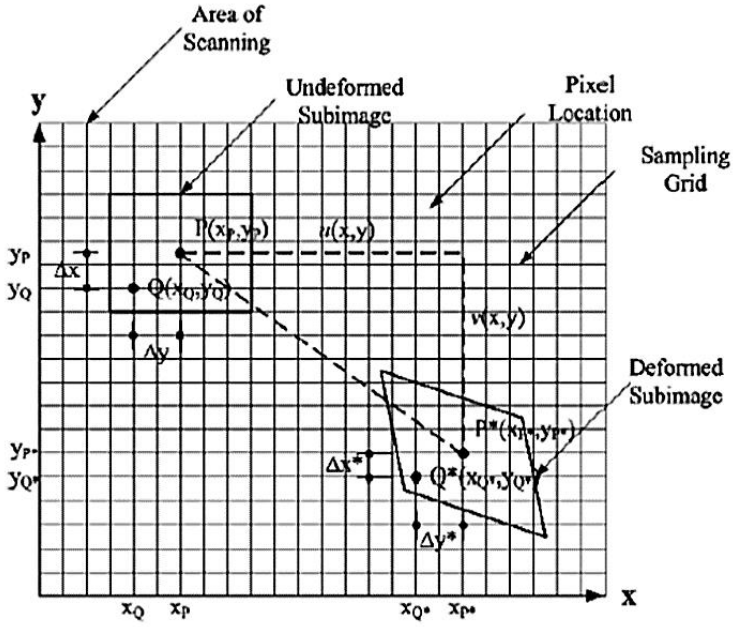

Figure 1. The Corresponding relation for distorted and undistorted tested-images [23]

Of importance, the DIC method, which relates to the grey scale correlation shown in Figure 2, requires at least two images of different experimental states for the investigated objects. The Camera images have converted to a grey scale image series according to the load changes. Then the images had analyzed to solve more sophisticate measuring tasks. High resolution or high-speed cameras need to be used. In this paper, high-resolution DSLR (Digital Single-Lens Reflex (the camera had been chosen to carry out this task.

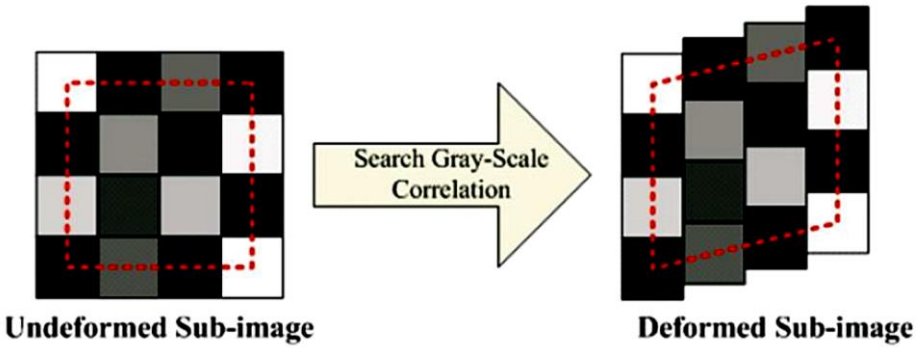

Figure 2. Gray-scale correlation between deformed and un-deformed sub-image [23]

The Pearson's linear correlation coefficient is considered in this work. Taking column *Xa* in form matrix *X* and column *Yb* in a form matrix *Y*, having means.

$$\bar{X}_a = \sum_{i=0}^{n}(x_{a,i})/n \text{ and } \bar{Y}_b = \sum_{j=1}^{n}(Y_{b,j})/n \quad (1)$$

Pearson's linear correlation coefficient *rho* (a, b) is defined as:

$$rho(a,b) = \frac{\sum_{i=1}^{n}(x_{a,i} - \bar{X}_a)(Y_{b,i} - \bar{Y}_b)}{\sqrt{\{\sum_{i=1}^{n}(x_{a,i} - \bar{X}_a)^2 \sum_{j=1}^{n}(Y_{b,i} - \bar{Y}_b)^2\}}} \quad (2)$$

Where *n* is the length number of each column.

The results of the achieved correlation coefficient range is from [–1, +1], and the value of –1 indicates a perfect negative correlation while the value of +1 indicates of a perfect positive correlation. The value of 0 shows there is no correlation between columns.

It is obvious that the successful usage of the above-mentioned correlation processes mainly depends on various parameters such as those mentioned below:

1. The contrast.
2. Speckle size of the scanned gray scale matrices patterns,
3. Subset matrix size,
4. Subset used shape functions
5. Digitization level of the gray scale values,

As shown in Figure 3. A speckle pattern had used and applied by using the spray white and black painting of the specimen surface.

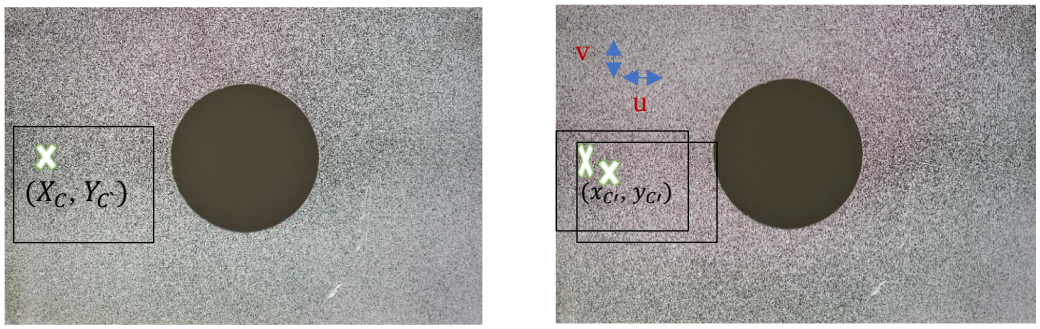

Figure 3. Reference image with an example of located subset and the deformed image with current subset location

Proceeding to the distortion of point *P*, this point has shifted to point P^*. The expression of this deformation is shown in Eq (3) and (4).

$$xP* = xP + u\,(x, y) \quad (3)$$

$$yP* = yP + v\,(x, y) \quad (4)$$

Where *(xP , yP)* and *(xP∗, yP∗)* are the coordinates of point *P* before and after distortion, respectively *u (x, y)* and *v (x, y)* are the shift functions in *x*- and *y*-direction separately. Finding the grayscale correlation coefficient will give the agreeing relationship between distorted and undistorted sub-images for estimating the distortion of sub-image as shown in Figure. 3. The correlation coefficient is represented in Eq. (2).

2.1. Calculation of strain and stress field

It is well-known that strain calculations and the relationship between the strain and displacements are described as a numerical differentiation process. In order to attain the strain estimation, the most straightforward estimation method is the differentiation of the calculated displacement fields. The numerical differentiation processing is listed as an unstable and/or risky process and should be undertaken with great caution because it might amplify the noise, especially at high-frequency levels. Strains are more difficult in term of resolving than the displacement fields because the strain field involves differentiation, which is quite sensitive to noise. This means any noise in the displacements field will magnify errors in the strain fields.

Now, to calculate the stress and strain field from the displacement field, the four points data after correlation need to be used, and for each point have displacement in X and Y direction which is represented as u and v subsequently. Hence these data are essential to compute the strain and stress numerically in advance. The equations which are used to get this aim and the theory are all taken from the reference textbook of finite element analysis, there are four points used to perform this computation. By using this method, the natural coordinates are used for two-dimensional domains are represented by ξ and η. Thus, the transformation will be carried out from *(x-y)* coordinates to *(ξ – η)* coordinates. Assuming there is a quadrilateral *ABCD* as shown in the Figure 4. The right shape with *A′ B′ C′ D′* indicates ξ, *η* which have value between -1 and +1 as shown in Figure 4.

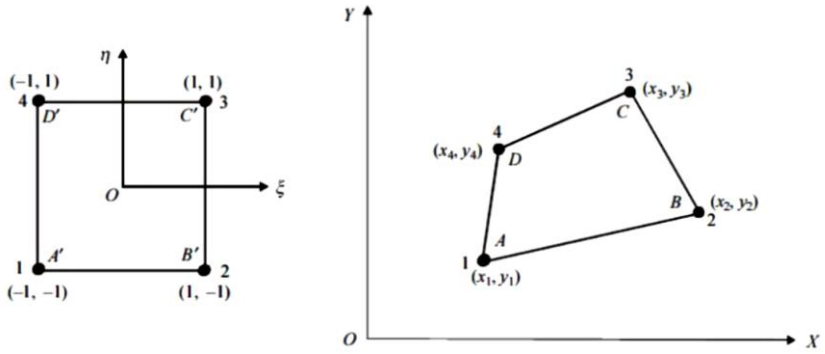

Figure 4. A general four-nodded quadrilateral element [24]

Under the assumption that P point within the element boundary, the displacements of this point extracted and/or interpolated by using the nodal displacements by using the shape functions for the above-shown element, which is name as an "isoperimetric element", and the displacements written as:

$$\begin{bmatrix} u \\ v \end{bmatrix} = \begin{bmatrix} N_1 & 0 & N_2 & 0 & N_3 & 0 & N_4 & 0 \\ 0 & N_1 & 0 & N_2 & 0 & N_3 & 0 & N_4 \end{bmatrix} \begin{bmatrix} u_1 \\ v_1 \\ u_2 \\ v_2 \\ u_3 \\ v_3 \\ u_3 \\ v_4 \end{bmatrix} \quad (5)$$

For this particular element and from Eq (9), this specific equation in FEM the Jacobian matrix, which had been involved in this work programming, is:

$$[J] = \begin{bmatrix} \sum \frac{\partial N_i}{\partial \xi} x_i & \sum \frac{\partial N_i}{\partial \xi} y_i \\ \sum \frac{\partial N_i}{\partial \eta} x_i & \sum \frac{\partial N_i}{\partial \eta} y_i \end{bmatrix} \quad (6)$$

For this look to the above quadrilateral element, the transformation is:

$$(x, y) \Longleftrightarrow f(\xi, \eta) \quad (7)$$

By consider P is considered as a point within the element in terms of nodal coordinates, the interpolation then can work like.

$$xp = \sum Ni\ xi \qquad yp = \sum Ni\ yi \quad (8)$$

Where i = 1, 2, …, which represent the number of nodes for the element equal 4 here)., considering *Ni* to be unity at node *i* and zero at all other remaining nodes, then the shape functions *Ni* can be written as

N_1 = (SF) (Equation of line 2-3) (Equation of line 3-4)

= (SF) (1-ξ) (1-η)

The SF had chosen such that at node, 1 is unity at lines 2-3 and 3-4 the shape functions values are considered to ensure that N_1 is zero at nodes 2, 3 and 4.

Which means at node 1, ξ = η = -1 and, therefore, SF=0.25 Thus our shape function is given by:

$$N_1 = (\frac{1}{4}) (1-\xi) (1-\eta) \quad (9)$$

The remaining shapes functions will be

$N_2 = (\frac{1}{4})\ (1+\xi)\ (1-\eta)$ (10)

$N_3 = (\frac{1}{4})\ (1+\xi)\ (1+\eta)$ (11)

$N_4 = (\frac{1}{4})\ (1-\xi)\ (1+\eta)$ (12)

The gained results from DIC written MATLAB program have been compared as well with the stress gained from Kirsch's equations that give the stress in any radial coordinates around the plate hole as shown in the Figure 5. Below:

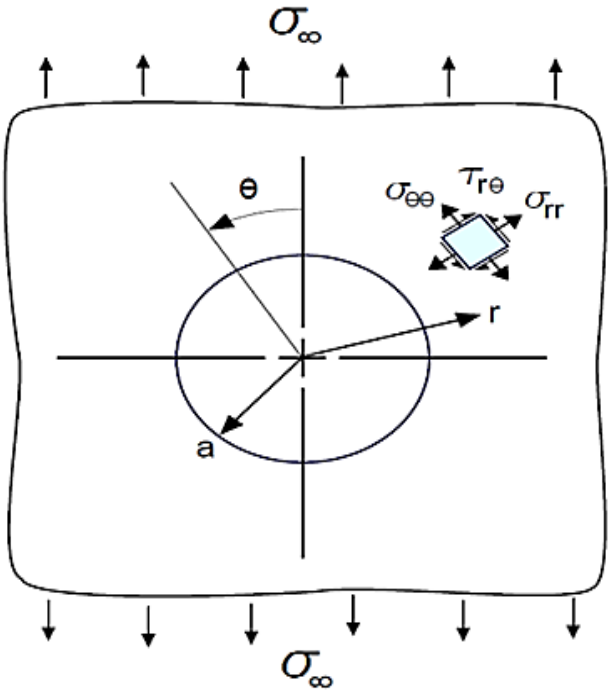

Figure 5. the Kirsch's equations parameters

Hence, the Kirsch's Equations are:

$$\sigma_{rr} = \frac{\sigma_\infty}{2}\left(1 - \left(\frac{a}{r}\right)^2\right) + \frac{\sigma_\infty}{2}\left(1 - 4\left(\frac{a}{r}\right)^4 + 3\left(\frac{a}{r}\right)^4\right)\cos 2\theta \quad (13)$$

$$\sigma_{\theta\theta} = \frac{\sigma_\infty}{2}\left(1 - \left(\frac{a}{r}\right)^2\right) - \frac{\sigma_\infty}{2}\left(1 + 3\left(\frac{a}{r}\right)^4\right)\cos 2\theta \quad (14)$$

$$\tau_{r\theta} = -\frac{\sigma_\infty}{2}\left(1 + 2\left(\frac{a}{r}\right)^2 - 3\left(\frac{a}{r}\right)^4\right)\sin 2\theta \quad (15)$$

As per the above figure, the σ_x and σ_y from DIC can be compared by taking the angle θ either 0 or 90°, so by taking the angle equal to zero the σ_{rr} will be equal to σ_x and $\sigma_{\theta\theta}$ will be equal to σ_y.

The percentage of accuracy of the obtained results is computed according to the following equation.

$$\eta = \left(1 - \left|\left(\frac{\text{Exact} - \text{DIC}}{\text{Exact}}\right)\right|\right) * 100 \quad (16)$$

2.2. DIC program approach

The code was built based on the DIC as a subset and finite element analyses. The formulation has provided results close to the ANSYS. The program was built to apply a "finite-element" DIC consideration as the basis for this study. By keeping similar DIC formulations to conduct the analysis of the experiments as the same numerical modelling (FEM).

The used code was based on "finite-element" theory by making quadrilateral element with four nodes and DIC algorithm. It is used to find and extract the nodal displacements for each picture and for each subsequently

loading step and this approach was used as fundamental in this study. The main input information that are forming all elements and nodes in the mesh.

The algorithm works to find the displacements, strain and stress, by taking the information for both of the reference image and deformed image with grayscale values, the data were obtained from both reference images and deformed images with grayscale values. Figure 6 shows the flowchart indicating the main parameters that the program used to initiate the correlation.

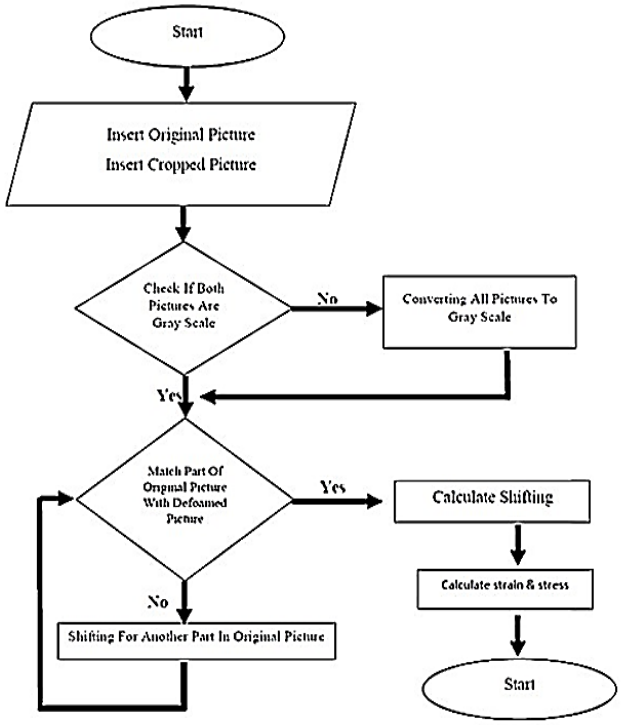

Figure 6. Flowchart for the written DIC program

3. Experimental settings

3.1. Tensile test

The explanation in the current section describes the preparation processes of tensile samples and, the procedure of measurement system, machinery, and the usage of X-Y camera setting system.

The entire plate dimension has specified in Table.1. each plate fixed by three bolts and jaw from the top and bottom of the tested plate.

Table 1. Plates dimension

Material	Plate height (mm)	Width (mm)	Hole / Notch (mm)	Thickness (mm)
Copper	109.21	153.84	45 mm hole	2.56
Aluminium	104.31	153.45	N/A	1.52

3.2. Experimental test rig

The main principles to get the deformation of the tested plates are through these steps that can be summarized as below:

i. The type of camera used in this experiment is NIKON (DSLR) D3200. To capture the series of the specimen images.

ii. During the entire experiment, each one of the two light sources was continuously provided as LED (Light Emitting Diode) sources that was directly illuminating the plate surface.

iii. Data monitoring to record the load number and monitor the behaviour of the plate.

The experimental rig was specially designed and manufactured to combine these three conditions and able to perform the tensile deformation. The experimental layout that was used to perform the testing of a 2D DIC application has shown in Figure 7.

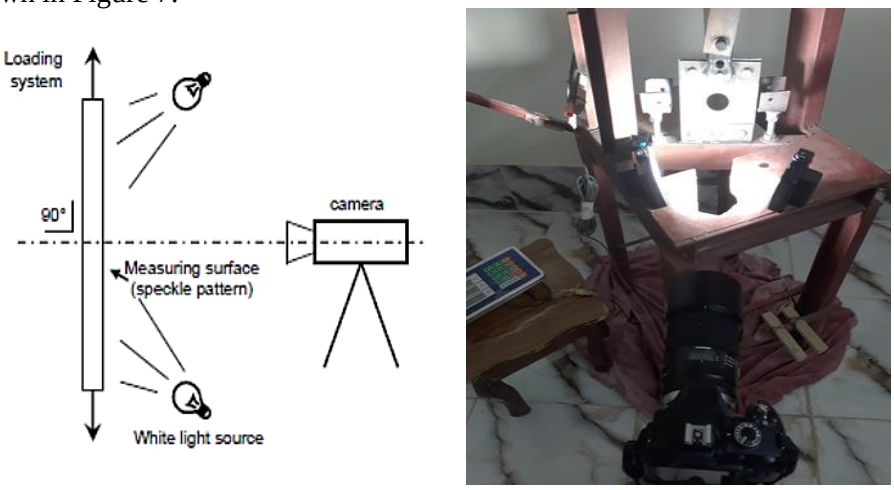

Figure 7. Testing layout

The flat specimen used in this experiment is mounted in a loading structure rig and with a pair of individual white lights. The DSLR camera stands on a tripod in front of the specimen. It captures one reference image before the test and series of images during the test. First, these images are checked, analyzed and correlated one after another to get the load increasing full-field strain maps. The main optical arrangement axis of the camera has to be in a direction perpendicular with respect to the plate surface. The working distance (which is defined between the target surface and the support of the cameras) was set about 0.66 mm.

3.3. The experimental procedures

The experimental work was carried out based on some theoretical calculations such as the position of the maximum tensile load that is applied on the plates to put the loading system on the right position. The test operation can be described in several steps as mention below:

i. Switch on the power from the power source to the LCD (Liquid-Crystal Display) load reader.

ii. Set the camera tripod in the horizontal ground level. Thus, there is no inclination angle. Later, the optical system was positioned to face the surface of the specimen.

iii. Switch on both LED lights and check the light distribution on the plate in the camera screen.

iv. Tight both chains enough. Thus, the loading process will be accurate.

v. Make the theoretical calculation to put the upper load limit.

vi. Record the load reading continuously with 100 kg interval.

4. Results and discussion

4.1 Aluminum plate in tension

The results obtained from the developed programs, other DIC software and exact analysis results are compared. The percentage of accuracy of the obtained results is computed according to the Eq (16).
For the cases where the exact results are not available, ANSYS results are used in Eq (16).
The results of plates that was analyzed by the built tensile rig are presented in this section. The analysis aims to obtain deformation, strains and stresses. Several types of plates with several conditions are considered for the analysis. A uniform plate under tension is analyzed. The plate is of 1.52 mm thickness and 153.45 X 104.31 mm width and height respectively. The plate is loaded by 25 KN is tension.
Exact results for stress and strain in loading direction for this case is

$$\sigma = \frac{P}{A} = \frac{25000}{153.45 * 1.52 * 10^{-6}} = 107.0095\ MPA \quad (18)$$

$$Since\ Young\ Modulus\ (E) = \frac{\sigma}{\varepsilon} \quad (19)$$

Thus, strain (ε) $= \frac{\sigma}{E} = \frac{107.0095 * 10^6}{70 * 10^9} = 1.5287 * 10^{-3}$ (20)

Table 2. Stress and strain results for plate without hole

σ with a percentage of agreement with the developed program		
Exact	**Developed Program**	**Ncorr**
107	**99.51 (93%)**	**/**
Strain with a percentage of agreement with the developed program		
Exact	**Developed Program**	**Ncorr**
$\mathbf{1.5287 * 10^{-3}}$	$\mathbf{1.36 * 10^{-3}}$ **(89%)**	$\mathbf{1.6 * 10^{-3}}$ **(96%)**

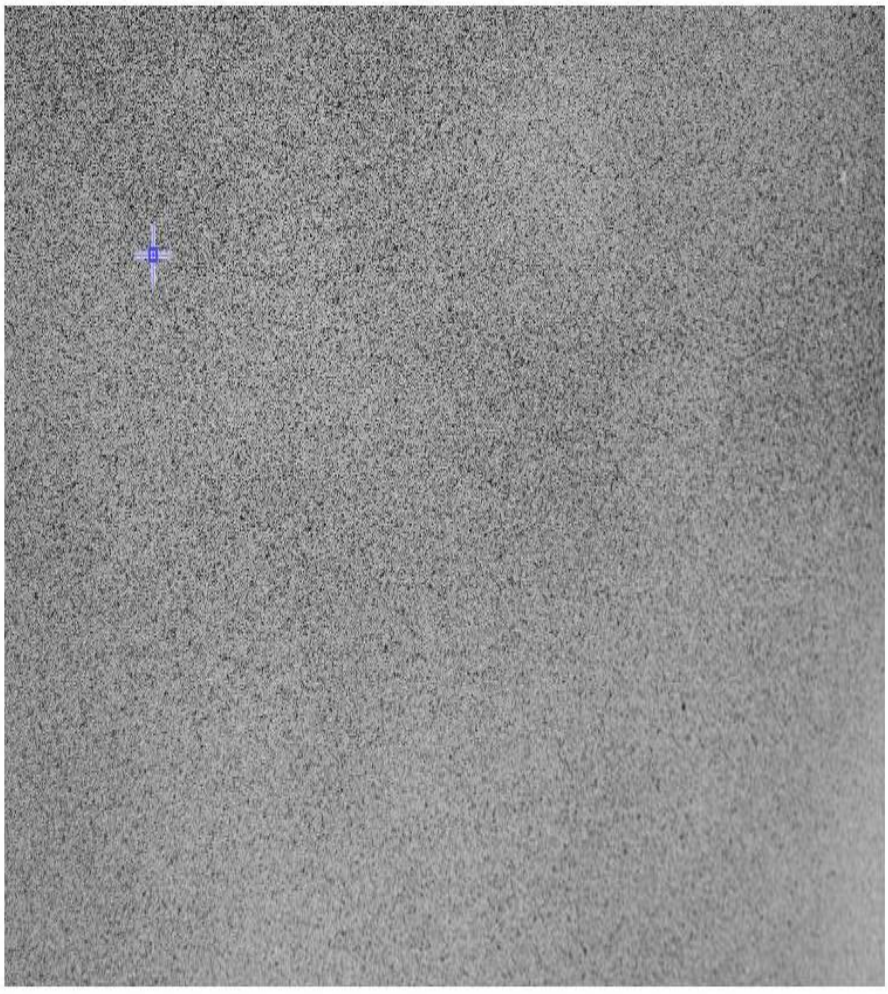

Figure 8. The point plotted by written DIC MATLAB program for case 1.

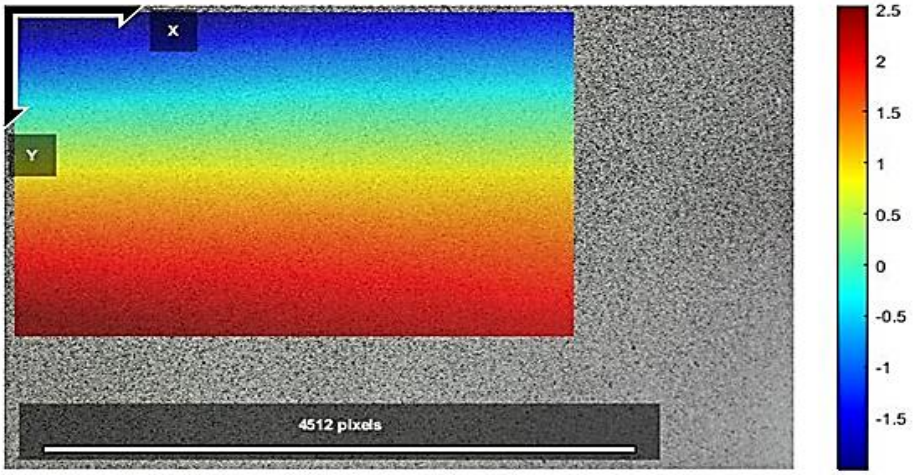

Type: v-plot
Reference Name: DSC_0021.JPG
Current Name: DSC_0023.JPG
Analysis type: regular
RG-DIC Radius: 20 | Subset Spacing: 3
Diffnorm Cutoff: 1e-06 | Iteration Cutoff: 50 | Threads: 4
Step Analysis: Disabled
RG-DIC Subset Truncation: Disabled
Image Correspondences: [0 1]
Units/pixels: 1 pixels/pixels
Correlation Coefficient Cutoff: 0.0739
Radial Lens Distortion Coefficient: 0
Max: 2.7680 pixels | Median: 0.8774 pixels | Min: -2.4371 pixels

Figure 9. Ncorr V displacements for the case 1

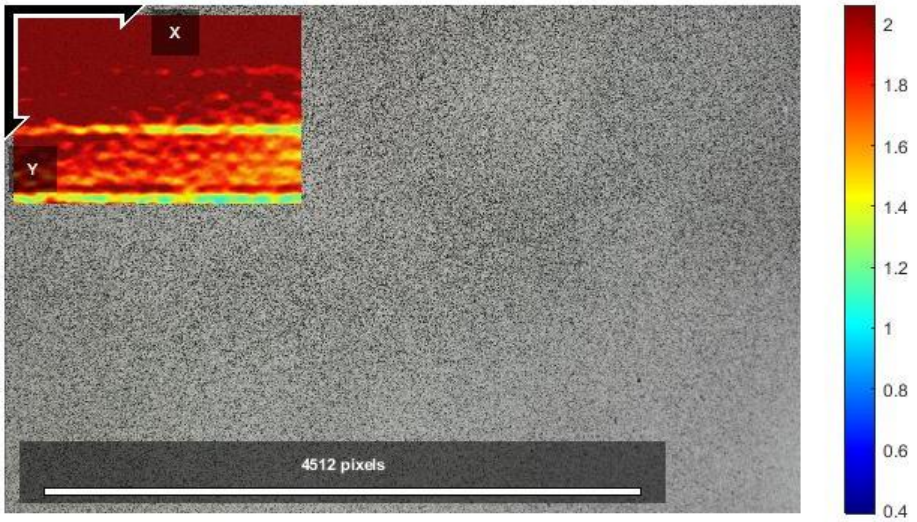

Type: eyy-plot
Reference Name: DSC_0021.JPG
Current Name: DSC_0023.JPG
Analysis type: regular
RG-DIC Radius: 20 | Strain Radius: 15 | Subset Spacing: 3
Diffnorm Cutoff: 1e-06 | Iteration Cutoff: 50 | Threads: 4
Step Analysis: Disabled
RG-DIC Subset Truncation: Disabled | Strain Subset Truncation: Disabled
Image Correspondences: [0 1]
Units/pixels: 1 pixels/pixels
Correlation Coefficient Cutoff: 0.0427
Radial Lens Distortion Coefficient: 0
Max: 0.0037 | Median: 0.0021 | Min: 0.0011

Figure 10. Ncorr results (strain (eyy)) for the aluminum without hole

The photos of the experiment of the plate are further analyzed by Ncorr for strains. A plate with a central hole in tension is analyzed for strains. The plate is made of copper with 2.56 mm thickness and 153.84 X 104.31 mm width and height respectively. The plate has a central circular hole with 45 mm diameter. The plate has subjected to 31750 N force by the built tensile rig. Photos have taken and analyzed by DIC using the built program Ncorr and ANSYS.

4.2. Copper plate with a hole

The results are compared with the analytical results (Kirsch's Equations (13-15). As shown in Figure 11, three points are selected for the analysis P1, P2 and P3. Coordinates of the points are as follows: P1: (0, 20) ; P2: (-20, 0) ; P3: (30, 0)

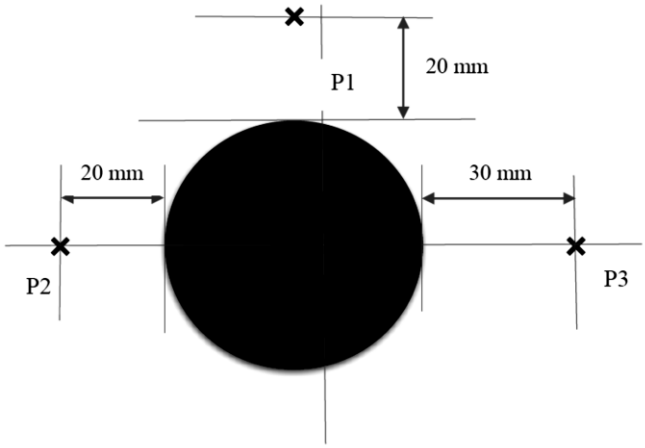

Figure 11. Analyzed plate with a circular hole

The analytical solution of stress in x-direction σ_x and y-direction σ_y for these points are obtained by substituting the following values of radial coordinates and angle value the Kirsch's Equations (13-15) : σ_∞ = 80.6184 MPa, By taking the P1 coordinates are r = 0.02 m and θ = 0, in Kirsch's Equations (13-15)

$$\sigma_{rr} = \frac{80.6184*10^6}{2}\left(1-\left(\frac{22.5*10^{-3}}{0.02}\right)^2\right)+\frac{80.6184*10^6}{2}\left(1-4\left(\frac{22.5*10^{-3}}{0.02}\right)^4+3\left(\frac{22.5*10^{-3}}{0.02}\right)^4\right) = 325.3 \text{ MPa} = \sigma_y \quad (21)$$

$$\sigma_{\theta\theta} = \frac{80.6184*10^6}{2}\left(1-\left(\frac{22.5*10^{-3}}{0.02}\right)^2\right)-\frac{80.6184*10^6}{2}\left(1+3\left(\frac{22.5*10^{-3}}{0.02}\right)^4\right) = 40.6 \text{ MPa} = \sigma_x \quad (22)$$

$$\tau_{r\theta} = -\frac{\sigma_\infty}{2}\left(1+2\left(\frac{a}{r}\right)^2-3\left(\frac{a}{r}\right)^4\right)\sin 2\theta = 0 \quad (23)$$

It should be mentioned that the analytical solution (Kirsch's Equations (13-15)) is limited for plate with infinite dimensions of width and height. Thus, it is not the exact solution for the analyzed plate in the current study, but it is considered for comparison. The problem is analyzed by finite element method using ANSYS 17 program, symmetry only quarter of the plate is considered for modelling. Symmetry, as shown in Figures 6-5 with element quad mesh type, is adopted in ANSYS, material properties is E= 128 GPa, v=0.33. By taking the results from the written program, the first thing that must be done is to take the code and pick up specific rectangle to make sure the comparison and the validity is working properly.

As mentioned above the validation radial coordinate have been considered with angle (r, θ) as (0, 0.02) by comparing ANSYS result with the results obtained from Eq (21) which gave the results as σ_x and σ_y.

The coordinates need to be transformed from metric to pixels and this is performed by using a MATLAB code by taking the actual measurement. The width equals 153.84 mm, and the width of the picture equals 6016 Pixels

$$\frac{Pixles}{mm} = \frac{6016}{153.84} = 39\ P/mm \quad (24)$$

Looking equation (24), it can be noticed that every 1 mm equal 39 pixels in. The coordinates, Thus, the pixels coordinates of this specific region MATLAB program is (2900, 375) the program requires the X location and Y location, the size of the rectangle that needs to be correlation processes work in and the number of squares need to be tested. Figure 12 is plotted by the developed program to perform the comparison.

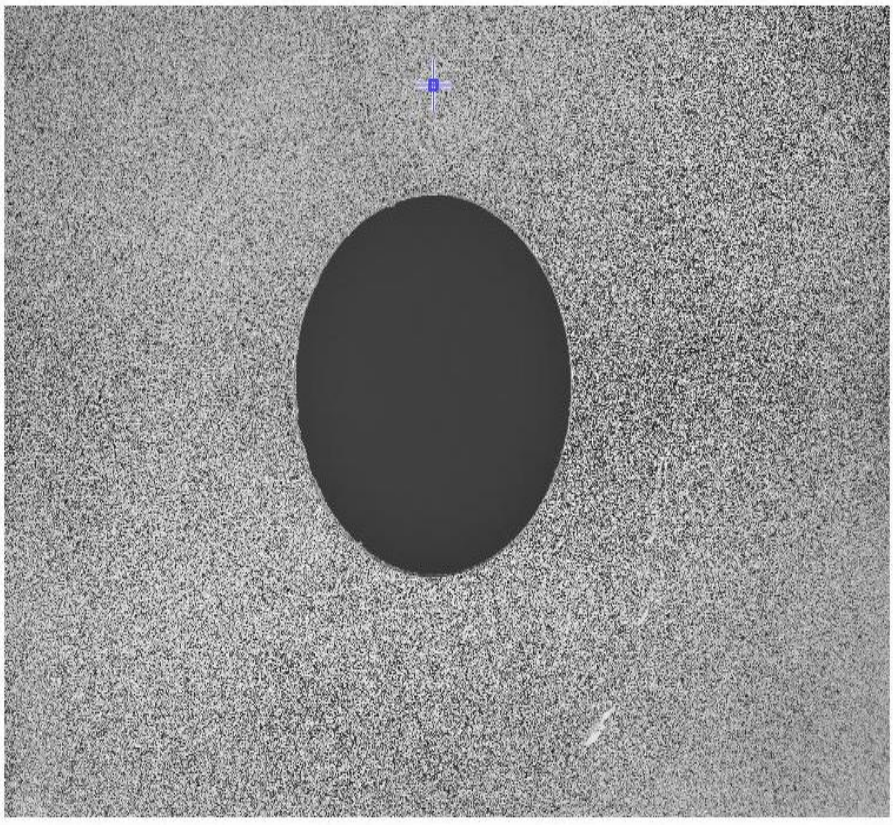

Figure 12. The point plotted by written DIC MATLAB program for the second case

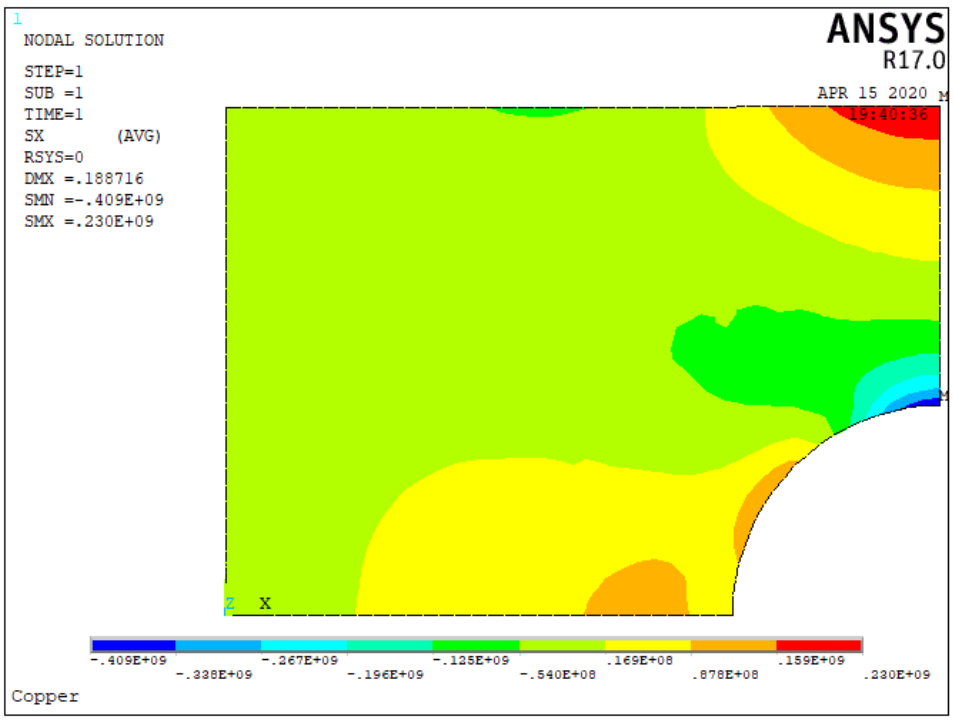

Figure 13. Ansys σ_x distribution for the second case

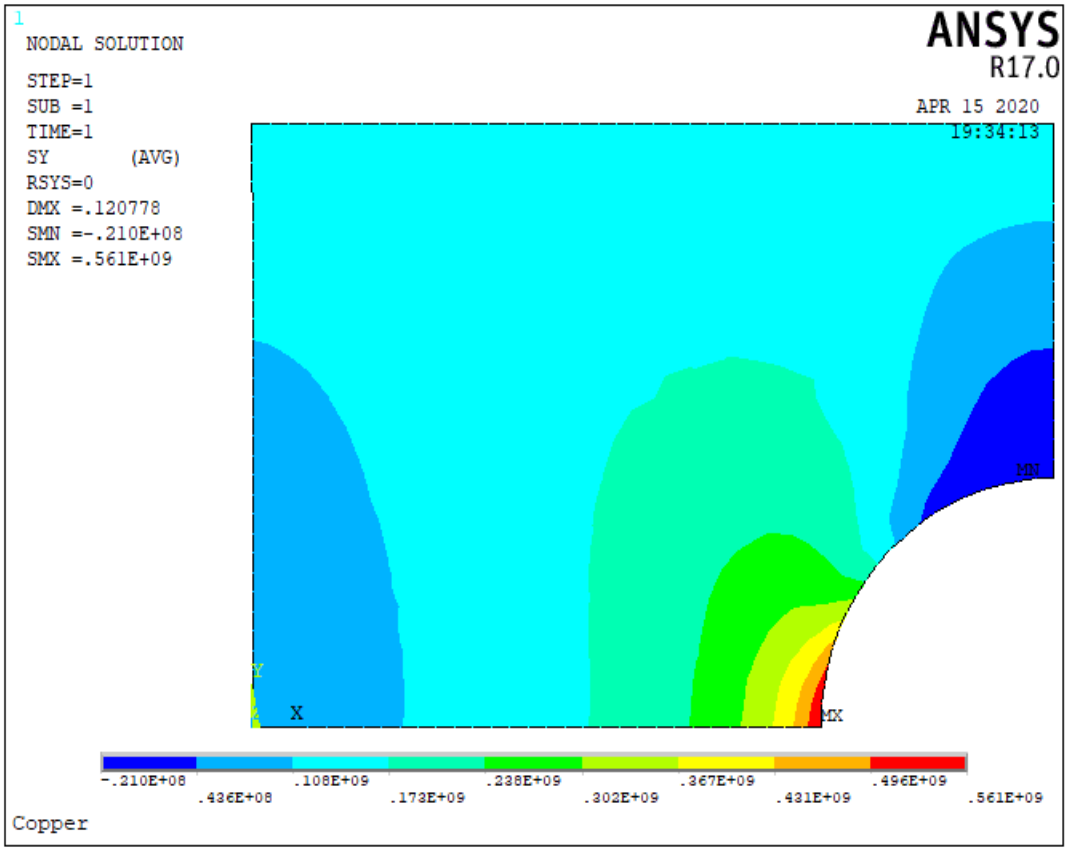

Figure.14. Ansys σ_y distribution for the second case

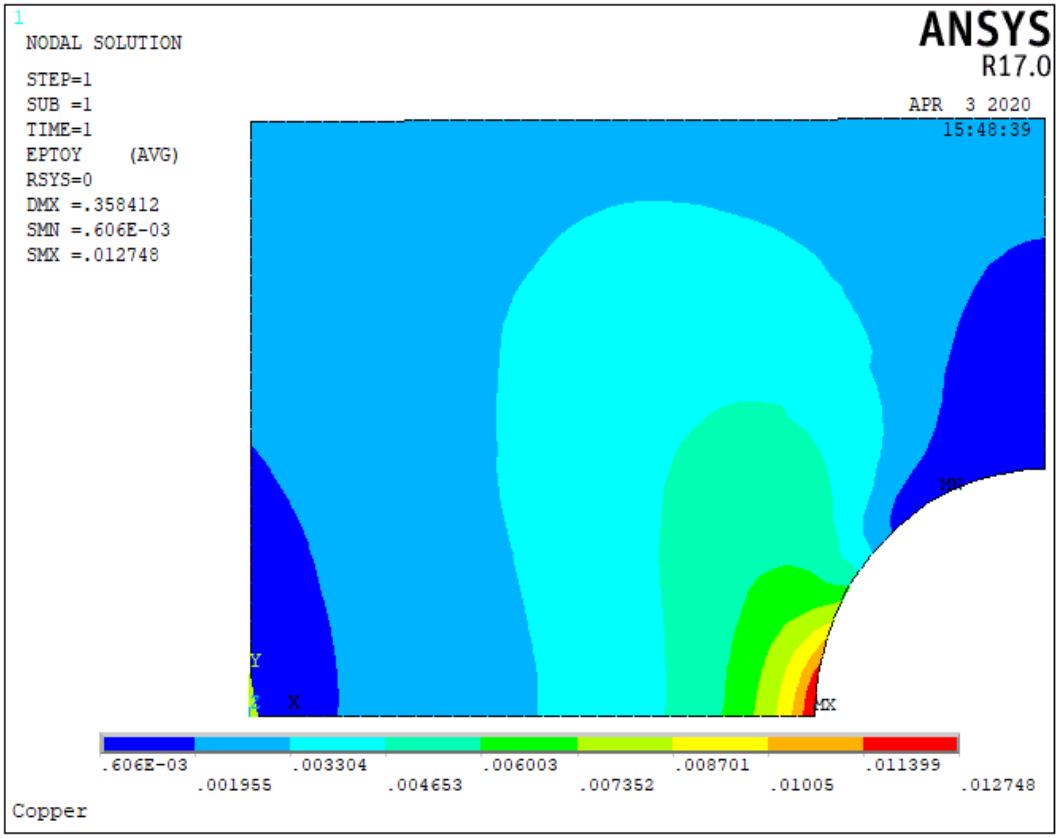

Figure 15. Ansys Strain (eyy) distribution for the second case

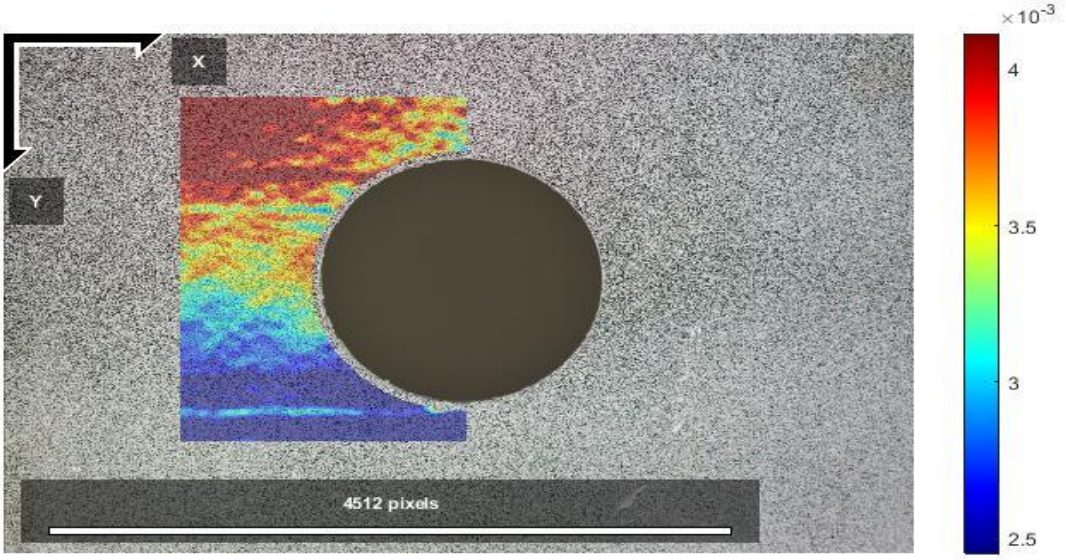

Type: eyy-plot
Reference Name: DSC_0001.JPG
Current Name: DSC_0009.JPG
Analysis type: regular
RG-DIC Radius: 20 | Strain Radius: 15 | Subset Spacing: 3
Diffnorm Cutoff: 1e-06 | Iteration Cutoff: 50 | Threads: 4
Step Analysis: Disabled
RG-DIC Subset Truncation: Disabled | Strain Subset Truncation: Disabled
Image Correspondences: [0 1]
Units/pixels: 1 pixels/pixels
Correlation Coefficient Cutoff: 0.1471
Radial Lens Distortion Coefficient: 0
Max: 0.0056 | Median: 0.0034 | Min: 0.0009

Figure 16. eyy Ncorr results for the second case

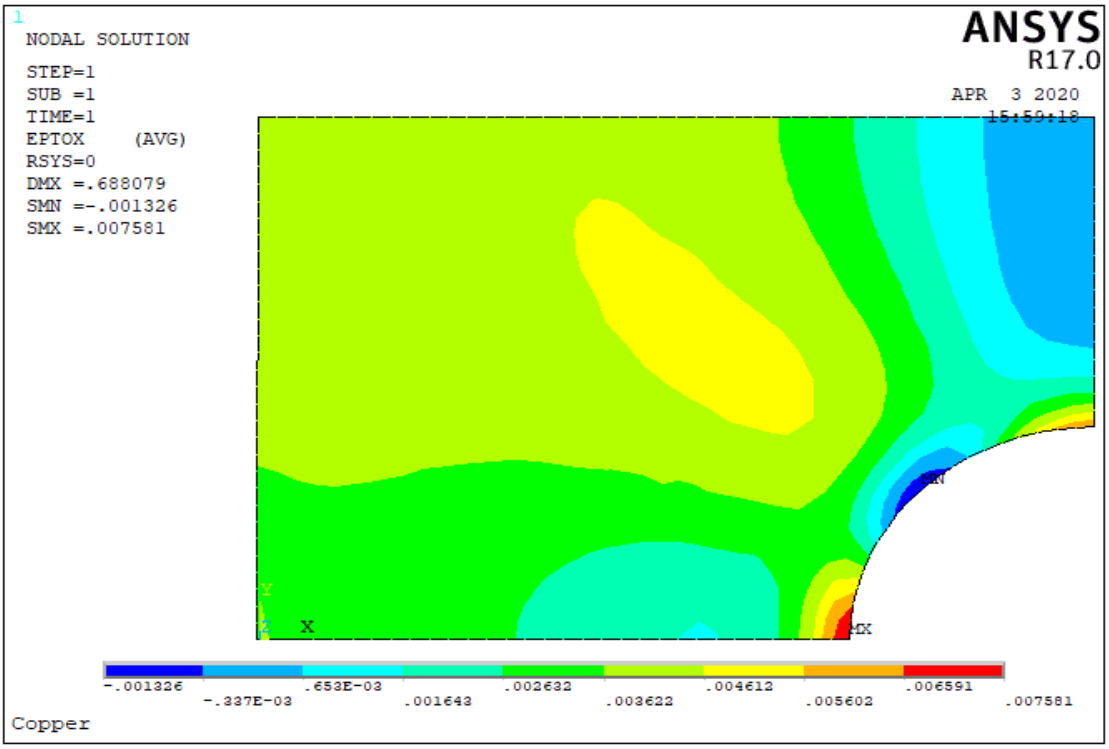

Figure 17. Ansys Strain (exx) distribution for the second case

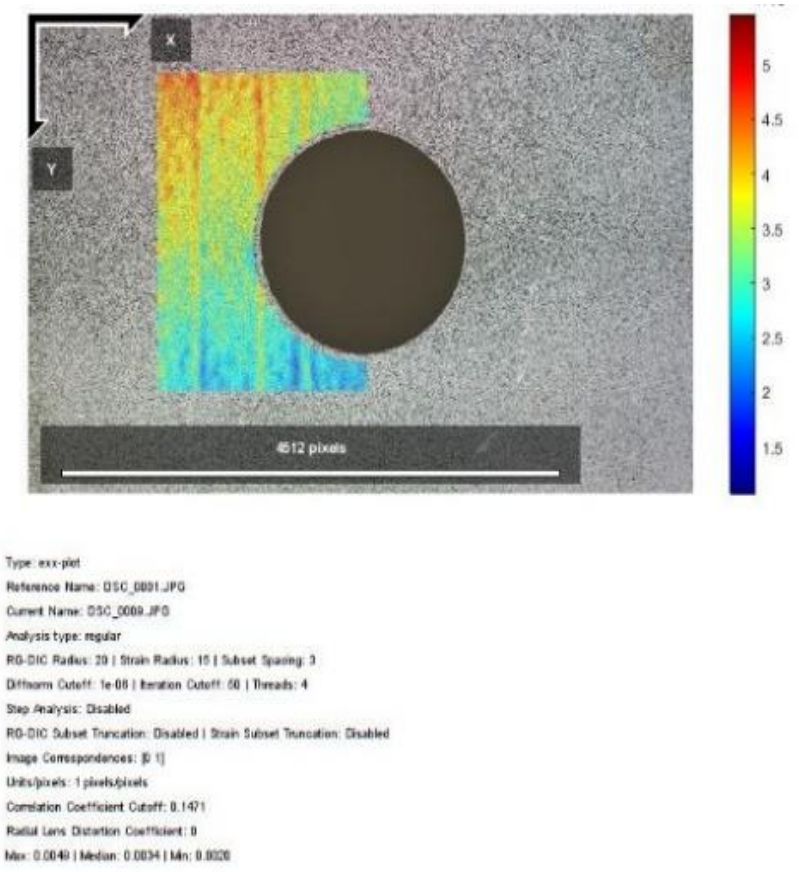

Figure 18. The exx Ncorr results for the second case

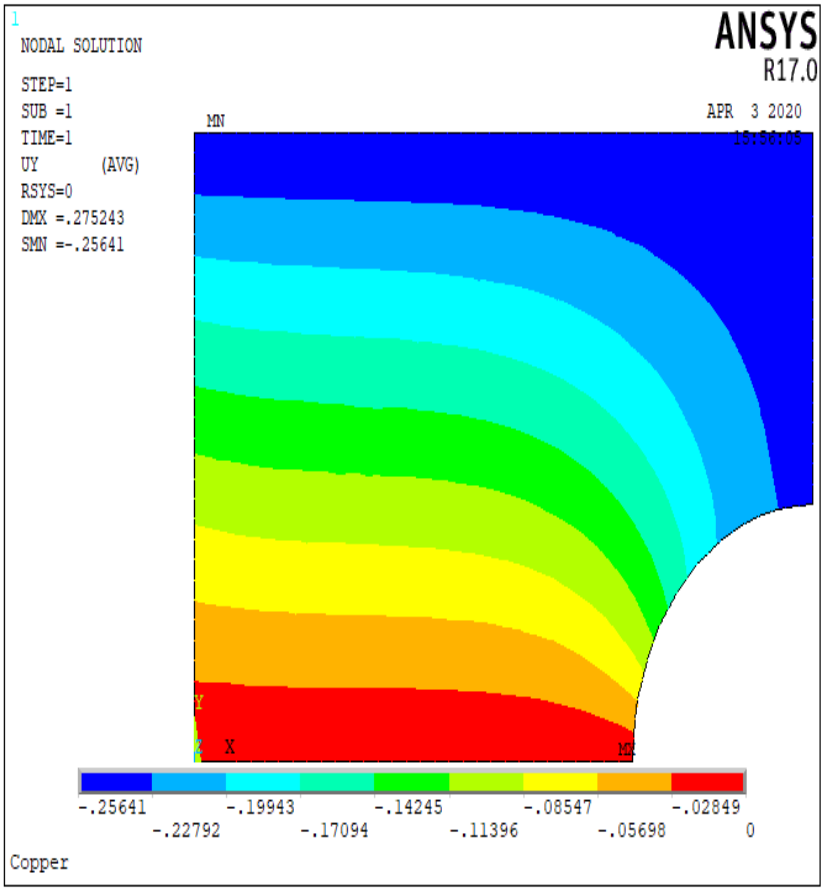

Figure 19. Ansys (V) Displacements distribution for the second case

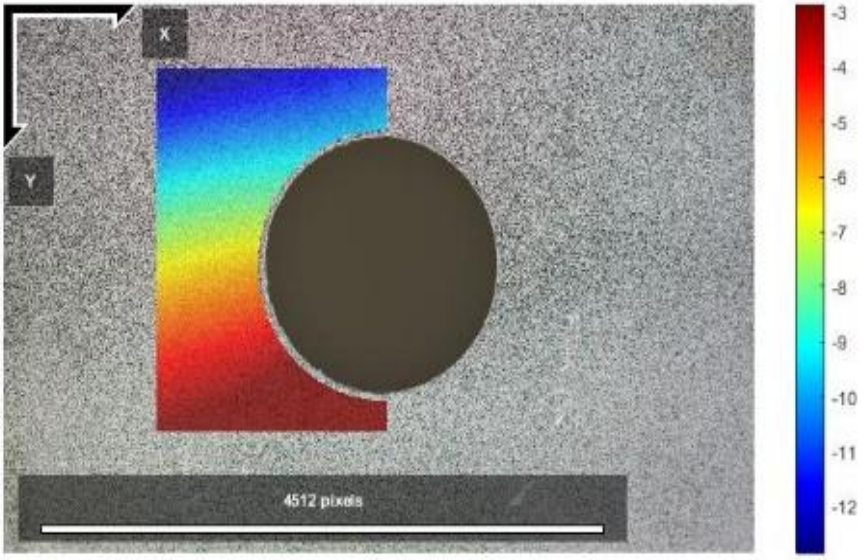

Type: v-plot
Reference Name: DSC_0001.JPG
Current Name: DSC_0010.JPG
Analysis type: regular
RG-DIC Radius: 20 | Subset Spacing: 3
Diffnorm Cutoff: 1e-06 | Iteration Cutoff: 50 | Threads: 4
Step Analysis: Disabled
RG-DIC Subset Truncation: Disabled
Image Correspondences: [0 1]
Units/pixels: 1 pixels/pixels
Correlation Coefficient Cutoff: 0.2478
Radial Lens Distortion Coefficient: 0
Max: -0.7080 pixels | Median: -7.3491 pixels | Min: -13.7488 pixels

Figure 20. The exx Ncorr results for the second case

Table 3. σ_x Results for plate with a circular hole

Point	Point Coordinates in mm (x,y) / in Pixles (x,y) / θ	σ_x(MPa) developed program	σ_x (MPa) Results with Percentage of agreement with the developed program	
			Analytical (Eq. 21)	Ansys
P1	**(-0.02,0) / (2900,3219) / θ = - 90**	**34.5**	**40.6 (85%)**	**41.64 (83%)**
P2	**(0,0.02) / (2900,375) / θ = 0**	**158.4**	**142.6 (88.9%)**	**134.3 (82%)**
P3	**(0.03,0) / (4700,1900) / θ = - 270**	**31.1**	**29.7 (92%)**	**31.4 (97.7%)**

Table 4. σ_y Results for plate with a circular hole

Point	Point Coordinates in mm (x,y) / in Pixles (x,y) / θ	σ_y(MPa) developed program	σ_y (MPa) Results with Percentage of agreement with the developed program	
			Analytical (Eq. 21)	Ansys
P1	**(-0.02,0) / (2900,3219) / θ = - 90**	**289.5**	**325.3 (89%)**	**339.3 (85%)**
P2	**(0,0.02) / (2900,375) / θ = 0**	**22.9**	**19.2 (80.7%)**	**20.1 (86%)**
P3	**(0.03,0) / (4700,1900) / θ = - 270**	**120.2**	**141.5 (85%)**	**134.6 (89%)**

Table 5. Strain (ε_x) results for plate with a circular hole

Point	Point Coordinates in mm (x,y) / in Pixles (x,y) / θ	ε_x developed program	ε_x Results with Percentage of agreement with the developed program	
			Ansys	Ncorr
P1	(0,0.02) / (2900,375) / θ = 0	$2.154 * 10^{-3}$	$2.367 * 10^{-3}$ (91%)	$2.9 * 10^{-3}$ (81%)
P2	(-0.02,0) / (2900,3219) / θ=90	$2.645*10^{-3}$	$2.814 * 10^{-3}$ (94%)	$3.2 * 10^{-3}$ (83%)
P3	(0.03,0) / (4700,1900) /θ=270	$2.289 * 10^{-3}$	$2.083* 10^{-3}$ (90%)	$2.5 * 10^{-3}$ (92%)

Table 6. Strain (ε_y) results for plate with a circular hole

Point	Point Coordinates in mm (x,y) / in Pixles (x,y) / θ	ε_y developed program	ε_y Results with Percentage of agreement with the developed program	
			Ansys	Ncorr
P1	(0,0.02) / (2900,375) / θ = 0	$1.92613* 10^{-3}$	$2.1642 *10^{-3}$ (89%)	$2.1 * 10^{-3}$ (91%)
P2	(-0.02,0) / (2900,3219) / θ=90	$4.466 * 10^{-3}$	$4.653 * 10^{-3}$ (96%)	$3.8 * * 10^{-3}$ (82%)
P3	(0.03,0) / (4700,1900) /θ=270	$2.322 *10^{-3}$	$2.638 * 10^{-3}$ (88%)	$2.91 *10^{-3}$ (80%)

Table 7. Displacements (v) results for plate with a circular hole

Point	Point Coordinates in mm (x,y) / in Pixles (x,y) / θ	Displacements (v) mm / developed program	$Displacements\ (v) mm$ Results with Percentage of agreement with the developed program	
			Ansys	Ncorr
P1	(0,0.02) / (2900,375) / θ = 0	0.20126	0.2164 (93%)	0.183 (90%)
P2	(-0.02,0) / (2900,3219) / θ=90	0.396	0.426 (92%)	0.3469 (84%)
P3	(0.03,0) / (4700,1900) /θ=270	0.0037	0 mm (99%)	0.076 (97%)

Tables 3-7 show that the results of the developed program provide satisfactory agreement with results obtained by other methods.

5. Conclusion and recommendations

The following major conclusions can be drawn from the present work:

- The advantage of using the proposed DIC system, it provides a remote way to measure displacements, strain and stress.
- The experiments performed have successfully fulfilled the given objectives. The experiments conducted in this paper has shown a successful agreement between the principles of tensile testing using exact solution results and the proposed DIC system.

- The proposed DIC system has successfully applied for tensile strain measurement. The measurement results demonstrate that DIC has a great potential for providing full-field strain measurement into the specimens.
- In tensile tests, the proposed DIC can measure strain at any point in the sample while the average strain has obtained with the traditional method.
- The novelty of this research is writing a MATLAB DIC code that presents an approach to perform fast, accurate and efficient DIC test. This approach involved manufacturing especial device to perform the testing of the specimen. The optical tool was a high-resolution DSLR camera to capture DIC images. The measurements on the plates were confirmed to be very effective with satisfactory uncertainties, both in displacements and strains.

Recommendations

- Using 3D DIC utilizing two digital cameras, which can be applied to test 3D object, and scale up this study to deal with various and complex states of loading.
- Using other image correlation methods such as DVC (Digital Volume Correlation) and evaluate their performance in relation to the method presented in this paper, the DIC.
- Comparing the results achieved from this technique with results achieved by other DIC global approaches.
- Considering the systematic error of the DIC results within the displacement and strain measurements due to the grey-level interpolation.
- Using the DIC technique to achieve Stress-Strain curves for various materials.

Acknowledgment

I would like to express my deep sense of gratitude and indebtedness to my Guide Prof and PG coordinator Dr. Zaid S. Hammoudi and Dr. Dhia Ahmed Salal, Department of Mechanical Engineering, University of Diyala, for their invaluable encouragement, suggestions and support from an early stage of this work and providing me extraordinary experiences throughout the work.

References

[1] C. Sun, D. W. Brown, B. Clausen, D. C. Foley, K. Y. Yu, Y. Chen, S. A. Maloy, K. T. Hartwig, H. Wang, and X. Zhang, "In situ neutron diffraction study on temperature dependent deformation mechanisms of ultrafine grained austenitic Fe–14Cr–16Ni alloy", *International Journal of Plasticity*, Vol. 53, pp. 125-134, 2014.

[2] E. Polatidis, N. Zotov, E. Bischoff, and E. J. Mittemeijer, "The effect of cyclic tensile loading on the stress-induced transformation mechanism in superelastic NiTi alloys: an in-situ X-ray diffraction study", *Scripta Materialia*, Vol.100, pp.59-62, 2015.

[3] L. Zhao, H. Jing, L. Xu, Y. Han, and J. Xiu, "Effect of residual stress on creep crack growth behavior in ASME P92 steel", Engineering *Fracture Mechanics*, Vol.110, pp.233-248, 2013.

[4] Ren, Zhigang, Meng Chen, and Weiguo Xu. "Dynamic mechanical property of hybrid fiber reinforced concrete (HFRC)", *Journal of Wuhan University of Technology-Mater. Sci. Ed.* 27, no. 4, pp.783-788, 2012.

[5] W. Woo, V. T. Em, E-Y. Kim, S. H. Han, Y. S. Han, and S-H. Choi. "Stress–strain relationship between ferrite and martensite in a dual-phase steel studied by in situ neutron diffraction and crystal plasticity theories." *Acta materialia*, Vol. 60, No. 20, pp.6972-6981, 2012.

[6] R.T. Smith, T. Lolla, D. Gandy, L. Wu, G. Faria, A.J. Ramirez, S.S. Babu and P.M. Anderson, " In situ X-ray diffraction analysis of strain-induced transformations in Fe-and Co-base hardfacing alloys", *Scripta Materialia*, Vol.*98*, pp.60-63, 2015.

[7] Yoneyama S, Murasawa G. Digital image correlation, experimental mechanics. Encyclopedia of Life Support Systems (EOLSS). Developed under the Auspices of the UNESCO, Eolss Publishers, Paris, France. 2009.

[8] M. Grediac, "The use of full-field measurement methods in composite material characterization: interest and limitations", Composites *Part A: applied science and manufacturing*, Vol. 35, No. 7-8, pp.751-761, 2004.

[9] N. L. J. McCormick, "“Digital Image Correlation,”," Materials Today, vol. 13(12), pp. 52-54, 2010.

[10] C. R. S. V, “Strain Measurements with the Digital Image Correlation System Vic-2D”, University of Colorado, Boulder, 2008.
[11] H. P. C. a. V. A. S, "“In-plane Strain Measurement by Digital Image Correlation”," Journal of the Brazilian Society of Mechanical Sciences and Engineering, vol. XXV, pp. 215-221, 2003.
[12] E. A. Cirne, "Full Field Strain Measurement During a Tensile Split Hopkinson Bar Experiment”," J. Phys. IV France,, Vols. Vol. 134, PP. 687 – 692, p. 687 – 692, 2006.
[13] J. J. Orteu, "3-D computer vision in experimental mechanics", Optics and Lasers in Engineering, France, 2007.
[14] S. Kut, "A Simple Method to Determine Ductile Fracture Strain in a Tensile Test of Plane Specimen’s," ISSN 0543-5846, vol. METABK 49 (4), pp. 295-299, 2010.
[15] S. Chakinala, "A Study of Algorithms Based on Digital Image Correlation for Embedding in a Full-Fiield Displacement Sensor with Subpixel Resolution," semantic scholar, 2013.
[16] A. S. V. Po-Chih Hung, "In-plane strain measurement by digital image correlation," Brazilian Society of Mechanical Sciences and Engineering, 2003.
[17 E. B. d. Assis, "Development of Digital Image Correlation tool to determine displacements," in *CILAMCE 2017*, Florianópolis, SC, Brazil, 2017.
[18] F. P. a. M. Grediac., "The Virtual Fields Method: Extracting Constitutive Mechanical Parameters from Full-field Deformation Measurements., Springer”, 2012.
[19] S. Cooreman., "Identification of the plastic material behaviour through full-field displacement measurements and inverse methods." PhD thesis, University of Brussels (VUB), 2008.
[20] M. E. A. Dost, "Cross correlation algorithms in digitized video images for object identification, movement evaluation and deformation analysis." Proceedings of SPIE, p. 5048., 2003.
[21] D. E. A. Vogel, J. of Electronic Packaging, Vol.124, pp. 345-351, 2002.
[22] P. Mazzoleni, Uncertainty estimation and reduction in digital image correlation measurements, PhD Thesis, Polytechnic University of Milan, 2013.
[23] P. Seshu, Textbook of Finite Element Analysis, New Delhi: Asoke K. Ghosh, 2012.